Probing dense granular materials by space-time dependent perturbations

L. Kondic
Department of Mathematical Sciences and Center for Applied Mathematics and Statistics, New Jersey Institute of Technology, Newark, New Jersey 07102, USA

O. M. Dybenko
Department of Mechanical Engineering, New Jersey Institute of Technology, Newark, New Jersey 07102, USA

R. P. Behringer
Department of Physics and Center for Nonlinear and Complex Systems, Duke University, Durham, North Carolina 27708, USA
(Received 14 May 2008; revised manuscript received 11 March 2009; published 13 April 2009)

The manner in which signals propagate through dense granular systems in both space and time is not well understood. In order to probe this process, we carry out discrete element simulations of the system response to excitations where we control the driving frequency and wavelength independently. Fourier analysis shows that properties of the signal depend strongly on the space-time scales of the perturbation. The features of the response provide a test bed for models that predict statistical and continuum space-time properties. We illustrate this connection between microscale physics and macroscale behavior by comparing the system response to a simple elastic model with damping.

DOI: 10.1103/PhysRevE.79.041304 PACS number(s): 45.70.−n, 43.40.+s, 46.40.Cd

I. INTRODUCTION

The issues of stress and energy transport in dense granular matter (DGM) are of significant importance in applications ranging from land mine detection to oil exploration, leading to a large body of research on the basic physical mechanisms involved. A major focus of recent work has been on the material response to static forces, typically involving small samples exposed to time-independent pointlike perturbations. A broad range of models has been proposed, including diffusive [1], wavelike [2–4], or elastic response [5]. Traditional continuum models [6,7] commonly assume an elastic or elastoplastic response. This collection of models is fundamentally at odds with each other, since the (possibly continuum limit) equations for these different descriptions are of parabolic, hyperbolic, or elliptic nature with respect to their spatial variables. Also important is the fact that a system response depends on the scale and the state of the system: wavelike response in static systems occurs on short (meso) scales, but elastic response on longer ones [5]. For dense systems, theory and experiment [5,8] suggest that an elastic description is best, but near jamming threshold, a hyperbolic description may apply [4].

Changing to dynamical processes adds a time scale, something that is not addressed in the works noted above. Hence, the questions that we seek to address are: in the presence of a time-dependent process, what is the nature of force transmission; what are the relevant time and length scales? The natural domain for probing these questions is sound propagation, which has been described by effective-medium approaches [7,9] where the motion is described by smooth local deformations. However, this approach is known to be incorrect in at least some situations [10] due to the local fluctuating (nonaffine) particle motion. We expect that nonaffine and other mesoscale phenomena will be manifested by a sensitivity to length and time scales for sound propagation. In order to probe both time *and* length scales, we inject signals at well-defined frequencies and with well-defined wavelengths in the work described here.

Separate control of spatial and temporal properties of the imposed signals is one of the distinguishing features of the presented results. This approach builds on a recent body of work where experiments and simulations use spatially uniform perturbations to probe pressure dependence of sound speed and the role of microstructure including force chains on signal propagation [10–13]. To put this in perspective, we note that very different issues arise for one-dimensional (1D) particle chains, which are characterized by nonlinear high-order wavelike continuum models [14]. An extension of these results to higher dimensions and realistic granular media remains to be carried out. Some of initial attempts to do so have been discussed recently in the context of land-mine detection [15].

In this paper we describe the response of DGM to space-time dependent perturbations with the goal of understanding relevant length and time scales for stress and energy transport. We concentrate on the regime where the imposed frequencies are low and the wavelengths are large compared to the particle size. We then compare results from discrete element (DEM) simulations to expectations based on a simple continuum picture that includes elastic and diffusive behaviors.

II. SIMULATIONS

We choose a relatively simple geometry in two spatial dimensions with grains contained between two rough walls (up-down) with periodic boundary conditions (left-right). The walls set the volume fraction, $\nu=0.9$. The particles are polydisperse disks with radii ranging over $\pm 5\%$ about the mean. For simplicity, we put gravity to zero. Particle-particle and particle-wall interactions are given by a soft-sphere model that includes damping, dynamic friction, and rota-

tional degrees of freedom (see, e.g., [16]). As appropriate for two-dimensional (2D) disks considered here, we use linear springs [17]. This model introduces the collision time, t_{col}, as one of the relevant time scales. Here, $t_{\mathrm{col}}=\pi/\sqrt{\omega_0^2-(\gamma_n/2)^2}$ and $\omega_0=\sqrt{2k_n/m}$, where k_n is the spring constant, m is the particle mass, and the damping γ_n is related to the restitution coefficient e_n by $\gamma_n=-2\ln(e_n)/t_{\mathrm{col}}$ [16]. The walls are made of particles that are rigidly joined, creating an impenetrable boundary. More detailed explorations of the influence of the DEM model parameters, or of the force model itself (e.g., presence of static friction), are considered elsewhere [18]; here we note that our preliminary results show only weak dependence of the response of the system on the details of the force model or on the parameters. For example, the influence of friction is very minor: the features of the results that follow are practically the same with or without frictional effects.

The system is prepared by very slow compression that is carried out by moving the upper wall from some initial position downwards until the required ν is reached. The particles are initially placed on a lattice and given random initial velocities. The compression is slow to ensure that no meaningful gradients of volume fraction or of the stresses remain in the system. It has been verified that the results that follow are independent of the preparation procedure. Then, after relaxing the system, the upper boundary is fixed and the lower boundary is perturbed by a standing-wave type of perturbation

$$z(x)=z_0+A\,\sin(\omega t)\sin(kx), \tag{1}$$

where $A, \omega=2\pi f$ and $k=2\pi/\lambda$ are the amplitude, angular frequency, and wave number.

The simulation parameters are as follows. The force constant in the particle interaction model is $k_n=k_f\bar{m}g/d$, where g is the acceleration of gravity and $\bar{m}$ and d are the average mass and diameter of a particle. To help interpretation we note that $k_f=4000$ (the value that we use here) corresponds approximately to the material properties of photoelastic disks used in [8]. The "system" particles that are allowed to move and the particles that build the oscillating wall are characterized by $e_n=0.9$ and by the coefficient of friction $\mu_s=0.1$. The upper wall particles are given $e_n=0.1$ and $\mu_s=0.9$. These (monodisperse) upper wall particles are made more frictional and inelastic in order to reduce reflection effects. The computation domain consists of 40 000 particles. The x dimension is $L=250d$; at the volume fraction of 0.9, the z dimension of the system is approximately $130d$. The imposed perturbation is characterized by the amplitude $A=0.6d$ and by varied frequency, f, and wavelength, λ. The frequency range is such that the following conditions are satisfied: $1/t_{\mathrm{col}}\ll f\ll c^*/d$, where c^* is the speed of sound in the solid. The considered wavelengths are much larger than the particle diameter. We use a large system so to reduce the boundary and finite-size effects. In addition, for the specified parameters, some key features are only visible in such a large system. This is also a reason for limiting our current analysis to 2D geometry.

Figure 1 shows a system snapshot just after activating the perturbation at the lower boundary. Colors show forces on

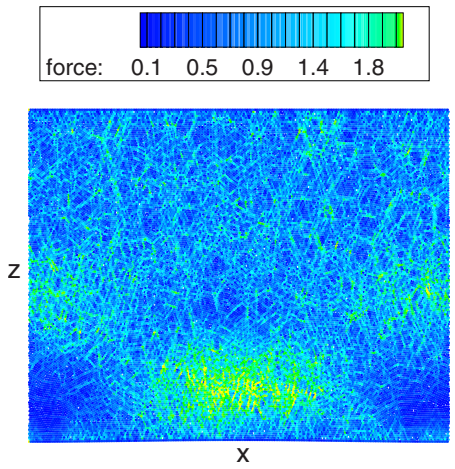

FIG. 1. (Color online) Snapshot of the simulation domain soon after perturbation of the lower boundary has been activated. The figure shows the forces (normalized by the mean) that the particle experience at a given time. The upper wall is static and the lower one performs standing-wave type of motion. 40 000 particles.

particles, with blue/dark corresponding to low and green-yellow/light to large forces. We note the force chains in the interior of the domain, as typically observed for DGM. We note that we have observed some rearrangements of the contacts between particles, especially close to the perturbation itself. However, we have not observed any significant differences in the main properties of signal propagation as A is modified, suggesting that this contact breaking and remaking is not crucial in determining the properties of propagating signal.

While force chain properties are of significant interest in understanding signal propagation in DGM (see, e.g., [12,13]), we focus here on quantities that can be averaged over a volume which is small compared to the system size, but that still contains relatively large number of particles; typically we use the network of 64×64 rectangular cells for spatial averaging. We also average over time intervals long compared to t_{col} but short compared to $1/f$. The results do not depend on the details of the averaging procedure for the conditions specified above.

We concentrate on the local elastic energy, E, defined as the cell average of the compression energies contained in the individual collisions taking place in a given cell during the specified time-averaging period. More precisely, elastic energy in a given cell l is defined by

$$E_l=\frac{1}{N_t\bar{n}_l}\frac{k_f}{2}\sum_{k=1}^{N_t}\sum_{j=1}^{n_l}\sum_{c=1}^{n_{c,j}}[x_{j,c}]^2, \tag{2}$$

where $x_{j,c}$ is the compression of particle j due to the collision c, normalized by the average particle diameter, d. Next, n_l is the number of particles in the cell l at a given time and $\bar{n}_l$ is the average number of particles during the period of $k=1$ to $k=N_t\gg1$ time steps (in practice, the averaging time scale is sufficiently short so that to a high degree of accuracy $n_l=\bar{n}_l$). Collisions may last over relatively long times, but even the fastest collisions are well resolved due to the short time step.

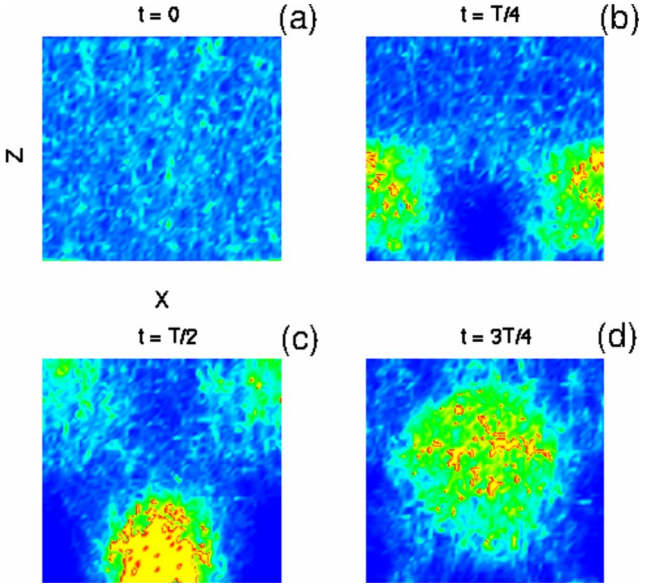

FIG. 2. (Color online) Energy fluctuations for a DEM simulation for a space-time harmonic perturbation ($\lambda=250d$ and $f=30$ Hz) applied at the lower boundary (yellow/light: high energy; blue/dark: low energy). Data in this figure are obtained by averaging over 64×64 subdomains.

We also define an average elastic energy in the cell l as

$$\langle E_l\rangle = \frac{k_f}{2} n_c \langle x_l\rangle^2 = \frac{k_f}{2} n_c \left[\frac{1}{N_t \bar{n}_l n_c} \sum_{k=1}^{N_t} \sum_{j=1}^{n_l} \sum_{c=1}^{n_{c,j}} x_{j,c} \right]^2, \qquad (3)$$

where $\langle x_l\rangle$ is the average compression per collision and n_c is the average number of collisions per particle. The averaging procedure is explained in more detail in [19], where it was also shown that for the systems characterized by large volume fraction, as considered here, the elastic energy dominates over the kinetic one.

Figure 2 shows E for different phases during one boundary oscillation [20]. We note well-defined waves propagating from the lower toward the upper boundary. The properties of these waves are the main focus of this work.

Figure 3 shows Fourier transforms (FTs), $E(z;f,\lambda)$, of E and of the elastic temperature, $T=\langle E\rangle^2-\langle E^2\rangle$ [19]. We give the dominant Fourier mode; spectral power data are similar. These results were obtained by carrying our Fourier expansion in the x direction of the cell-averaged data and then time averaging over many (typically 30) perturbation periods, thus increasing the signal-to-noise ratio. The transient behavior is eliminated by discarding the data obtained during the first few periods. We further verify the steady nature of the results by carrying out selected simulations for much longer times.

Figure 3 shows a well-defined propagation in the z direction. Clearly, E and T, which measures local deviations of E from the mean, follow each other closely. One important question is whether the system-selected wavelengths in the z direction depend on the system size. To answer this question, we have carried out simulations where both the domain size and λ are halved in the x direction (therefore equal to $125d$)

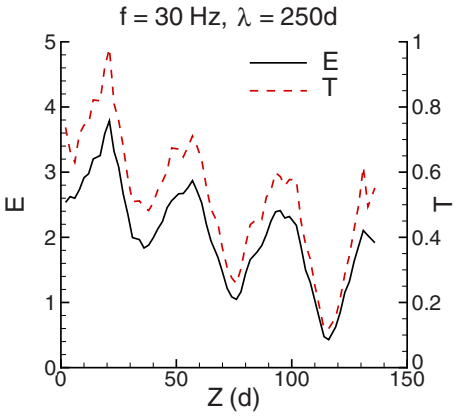

FIG. 3. (Color online) Dominant Fourier mode (the one imposed by the boundary motion) of the elastic energy and temperature (arbitrary units) as a function of z, the distance from the oscillating wall.

and then the results compared to the simulations where $L=250d$ and $\lambda=125d$. Similarly, we have carried out simulations where we increased the size of the domain in the z direction (leading to simulations with approximately 50 000 particles). In both cases, we have found that the results are independent of the system size, as long as the dimensions are sufficiently large, as is the case with the simulations presented here.

Figure 4, giving $E(z;f,\lambda)$ as λ and f are varied, homes in on the relevant scales. Figures 4(a) and 4(b) show that decreasing λ causes significant dispersion: the signal ceases to be wavelike and the length-scale information from the perturbation is lost. We note that the smaller λ's are still large compared to a particle size. Figures 4(c) and 4(d) show that increasing f also leads to the signal loss. For smaller f, the signal is weaker and characterized by a larger z-direction wavelength compared to Fig. 3. Thus, well-defined signal

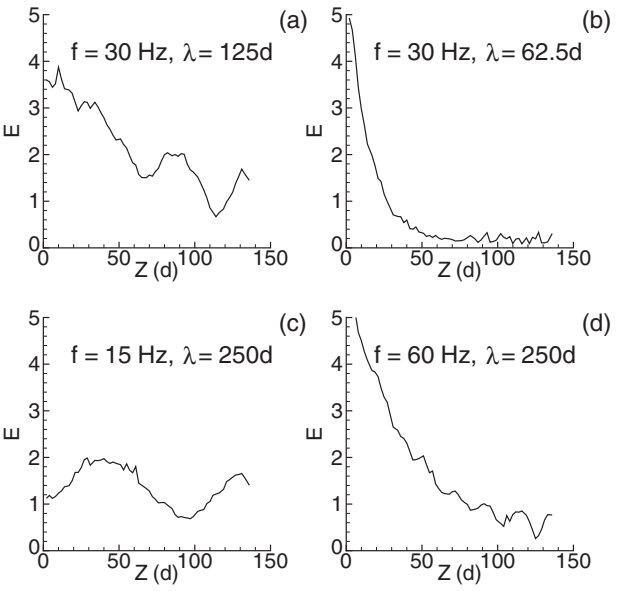

FIG. 4. Dominant Fourier mode of the elastic energy as the frequency and wavelength of the perturbation are modified.

propagates only in a narrow band of f's and λ's. For even smaller f's, the energy input is insufficient to trace accurately. We note that we have also carried out simulations with an effectively infinite λ, yielding a propagation speed consistent with previous work concentrating on similar systems [13].

III. CONTINUUM MODEL

We next compare these results to a model which includes elastic behavior and diffusive damping. We chose such a model since static force transmission well-above jamming densities is, to date, best described in terms of an elastic picture [5,8] and because we expect dissipative processes. Future work should consider other possible models which may be appropriate close to jamming transition or on shorter length scales, as discussed in Sec. I. Assume that the space-time properties of E (but similarly for pressure, temperature, or a component of the stress tensor) are given by

$$\nabla^2 E - \frac{1}{c^2}\frac{\partial^2 E}{\partial t^2} - \frac{1}{D}\frac{\partial E}{\partial t} = 0, \tag{4}$$

which as $D \to \infty$ becomes a linear wave equation often used to describe wave propagation in elastic solids and as $c \to \infty$ a diffusion equation. A diffusion model was used to describe signal propagation as a result of spatially uniform perturbations, although typically for much larger frequencies of driving [11]. In the present context, we emphasize that the model specified by Eq. (4) is not meant as a full description of the data, but only as a basis for comparison.

Equation (4) is given in a nondimensional form obtained by choosing L as a length scale and $1/\omega_p$ as a time scale, where ω_p is some typical imposed frequency (we use $\omega_p = 2\pi f_p$, $f_p = 30$ Hz). We take the diffusion D and the speed of propagation, c, as constants. Further assuming plane-wave solution as a zeroth order approximation to more complex waves that can be expected in DGM [13,14,21] in the form

$$E(x,z,t) = E_0 e^{\imath\omega t} e^{\imath kx} e^{\imath qz}, \tag{5}$$

one obtains the following dispersion relation:

$$q = -|q| e^{\imath\phi/2}, \quad |q^2| = \mathcal{X}^2 + (\omega/D)^2, \quad \tan\phi = -\frac{\omega}{(D\mathcal{X})}, \tag{6}$$

where $\mathcal{X} = (\omega/c)^2 - k^2$. We first discuss general features of such a mode in light of the simulation results and note that the results outlined below apply for a wide range of (constant) c's and D's. The following predictions are easily verified:

(i) For a fixed frequency of perturbation f, an increase of k leads to an increase of the dominant wavelength of the propagating signal, in agreement with Figs. 3 and 4(a).

(ii) Still for a fixed f, an increase of k also leads to larger $\mathrm{Im}(q)$ showing that stronger attenuation is expected for shorter λ's, in agreement with Figs. 3, 4(a), and 4(b).

(iii) For a fixed k, as f is decreased, one expects longer emerging wavelengths, in agreement with Fig. 4(c).

We note here that, while the attenuation of a propagating signal as a function of driving frequency has been considered before [11,13], we are not aware of any results discussing the dependence of attenuation on the spatial scales introduced by the perturbation. One feature of the DEM results which is not explained well by the model is the fact that Eq. (4) predicts essentially constant attenuation for larger f's, while in Fig. 4(d) we see stronger attenuation than, e.g., in Fig. 3, consistent with previous work [11,13]. One explanation for this difference is that the model predicts shorter emerging wavelengths for these high frequencies. These shorter wavelengths may become comparable to the particle size, where a continuum model is not expected to apply.

After finding reasonable agreement between the model, Eq. (4), and the simulations, we next ask whether the values of D and c deduced by comparison to the DEM data are in qualitative agreement with the commonly used ones. For this purpose, we extract the value of q from Fig. 3 and using the dispersion relation, Eq. (6), obtain $c \approx 0.025$ and $D \approx 0.01$. Similar values of c and D can be extracted from the results shown in Fig. 4 and from additional simulations using other values of f and λ (not shown), typically with the spread of obtained values of D larger than the one for c. The value of c can now be compared to the speed of sound resulting from elasticity theory

$$c* = \sqrt{E_y/[(1-\sigma^2)\rho]}/(L\omega_p), \tag{7}$$

where E_y, σ, ρ are the Young modulus, Poisson ratio, and density of the material. These material parameters can be extracted from the DEM force model [16], giving $c/c* \approx 0.1$, in general agreement with work [12].

An interpretation of D is more complicated. An estimate based on the particle size and some typical shear rate, such as average velocity gradient, underestimates significantly the predicted value of D, suggesting that a different mechanism is in place. Alternatively, we recall the estimate $D \approx v_e \ell/3$, where v_e is the velocity of energy transport and l is the transport mean-free path, measuring the distance traveled before the direction of propagation is randomized; for further discussion regarding applicability of this concept to dense granular materials, see, e.g., [9,11]. Let us assume that $v_e \approx c*$. The value of D predicted by the model then gives ℓ corresponding to $30-40d$. It will be of interest to analyze whether such a long length scale may be related to the correlation length introduced by the force-chain structure, an issue which has been a subject of considerable discussion [11–13,22]. It will be also of interest to explore how ℓ (and therefore D) varies with, e.g., the volume fraction or the imposed frequency. An additional task will be to analyze the influence of dimensionality of the system, since it has been suggested that in three-dimensions (3D) the correlation length of the force network may be much shorter [11]. We note in passing that, in the regime considered here, a diffusion model that was successfully applied to a 3D system driven at high frequencies [11] could not explain the main features of the DEM results presented in Figs. 3 and 4.

IV. CONCLUSION

In this work, we have considered response of a dense granular system to space-time dependent perturbations. This response turns out to strongly depend on the properties of perturbations and provides significant insight regarding the manner in which energy propagates. For the system considered here, we find that a reasonably good description of energy propagation can be reached via a simple linear wave equation with dissipation. This finding is perhaps not surprising, since it is known that elastic (with respect to spatial coordinates) models describe well the response of *static* granular systems. In this work, we show that similar behavior may be expected in a system exposed to continuous time-dependent perturbations where some amount of relative motion of the particles is present.

While we find consistent results between the simulations and the simple continuum model encouraging, we note that much more work is needed. Regarding simulations, we have considered propagation for a given volume fraction, therefore not considering explicitly the pressure dependence of the speed of propagation. For smaller volume fractions (closer to the jamming threshold) the nature of the signal propagation may be modified and it remains to be seen how the continuum model used here would apply in that case.

Regarding the continuum model itself, although we find that it describes well many features of the DEM results, better understanding of the attenuation properties of the signal is needed. The degree of agreement with the simulations suggests that for more precise comparisons one may need to consider frequency-dependent D. The question of coupling of different spatial and temporal scales needs to be considered as well.

We hope that probing DGM with both space and time dependent perturbations, as done here, will be utilized in future theoretical and particularly experimental efforts to build a more complete picture regarding stress and energy transport in dense granular matter.

ACKNOWLEDGMENTS

This work was supported by NSF under Grants No. DMS 0605857, No. 0835611, and No. DMR 0555431.

[1] S. N. Coppersmith, C.-h. Liu, S. Majumdar, O. Narayan, and T. A. Witten, Phys. Rev. E **53**, 4673 (1996).
[2] J. P. Bouchaud, M. E. Cates, J. R. Prakash, and S. F. Edwards, J. Phys. I **4**, 1383 (1994).
[3] M. Otto, J.-P. Bouchaud, P. Claudin, and Socolar, Phys. Rev. E **67**, 031302 (2003).
[4] R. Blumenfeld, Phys. Rev. Lett. **93**, 108301 (2004).
[5] C. Goldenberg and I. Goldhirsch, Nature (London) **435**, 188 (2005).
[6] R. M. Nedderman, *Statics and Kinematics of Granular Materials* (Cambridge University Press, Cambridge, England, 1992).
[7] J. D. Goddard, Proc. R. Soc. London, Ser. A **430**, 105 (1990).
[8] J. Geng, G. Reydellet, E. Clément, and R. P. Behringer, Physica D **182**, 274 (2003).
[9] P. Sheng, *Introduction to Wave Scattering, Localization, and Mesoscopic Phenomena* (Academic, New York, 1995).
[10] H. A. Makse, N. Gland, D. L. Johnson, and L. M. Schwartz, Phys. Rev. Lett. **83**, 5070 (1999).
[11] X. Jia, Phys. Rev. Lett. **93**, 154303 (2004).
[12] E. Somfai, J. N. Roux, J. H. Snoeijer, M. van Hecke, and W. van Saarloos, Phys. Rev. E **72**, 021301 (2005).
[13] S. R. Hostler and C. E. Brennen, Phys. Rev. E **72**, 031303 (2005).
[14] V. Nesterenko, *Dynamics of Heterogenous Materials* (Springer, New York, 2001).
[15] S. Sen, T. R. K. Mohan, D. P. Visco, S. Swaminathan, A. Sokolow, E. Avalos, and M. Nakagawa, Int. J. Mod. Phys. B **18**, 29516 (2005).
[16] L. Kondic, Phys. Rev. E **60**, 751 (1999).
[17] K. L. Johnson, *Contact Mechanics* (Cambridge University Press, Cambridge, 1989).
[18] L. Kondic and R. P. Behringer (unpublished).
[19] L. Kondic and R. P. Behringer, Europhys. Lett. **67**, 205 (2004).
[20] L. Kondic, http://m.njit.edu/~kondic/granular/signal/signal.html
[21] S. Sen, M. Manciu, R. S. Sinkovits, and A. J. Hurd, Granular Matter **3**, 33 (2001).
[22] C. H. Liu and S. R. Nagel, Phys. Rev. Lett. **68**, 2301 (1992).